sustainability

MDPI

Article

Comparative Thermal Performance Analysis of Coaxial Versus Conventional Pipes in District Heating Distribution Systems

Natalia Nuño-Villanueva, Ignacio Martín Nieto, Cristina Sáez Blázquez *, Enrique González-González, Miguel Ángel Maté-González, Víctor Pérez Fernández, Arturo Farfán Martín and Diego González-Aguilera

Department of Cartographic and Land Engineering, Higher Polytechnic School of Avila, University of Salamanca, 05003 Avila, Spain; id00816629@usal.es (N.N.-V.); nachomartin@usal.es (I.M.N.); egonzalezgonzalez@usal.es (E.G.-G.); mategonzalez@usal.es (M.Á.M.-G.); vperez@usal.es (V.P.F.); afarfan@usal.es (A.F.M.); daguilera@usal.es (D.G.-A.)

* Correspondence: u107596@usal.es

Abstract: District heating systems play a pivotal role in providing efficient and sustainable heating solutions for urban areas. In this sense, district heating systems that use geothermal resources have been gaining prominence in recent years, due to the non-intermittent nature of their application, among many other reasons. The present study investigates the thermal performance of novel coaxial pipes in comparison to conventional pipes within district heating distribution networks supplied by geothermal energy. Through experimental simulation and analysis, key thermal parameters such as heat transfer efficiency, thermal losses, and overall system effectiveness are evaluated through laboratory tests developed on a scale model. Experimental analysis concludes that, at a laboratory scale, heat energy efficiency can be improved by around 37% regarding the traditional geothermal distribution network. This improvement translates into a significant economic and environmental impact that has a direct influence on the viability of this type of system in different application scenarios. The results highlight the potential benefits of coaxial pipe designs in enhancing heat transfer efficiency and minimizing thermal losses, thus offering insights for optimizing geothermal district heating infrastructure for improved energy efficiency and sustainability. The novelty of this study lies in the innovative design and experimental validation of coaxial pipes, which demonstrate a 37% improvement in heat energy efficiency over conventional pipe designs in geothermal district heating systems, offering a breakthrough in optimizing heat transfer and minimizing thermal losses.

Keywords: district heating; geothermal energy; thermal efficiency; pipeline

Citation: Nuño-Villanueva, N.; Martín Nieto, I.; Sáez Blázquez, C.; González-González, E.; Maté-González, M.Á.; Fernández, V.P.; Farfán Martín, A.; González-Aguilera, D. Comparative Thermal Performance Analysis of Coaxial Versus Conventional Pipes in District Heating Distribution Systems. *Sustainability* **2024**, *16*, 10093. https://doi.org/10.3390/su162210093

Academic Editor: Paulo Santos

Received: 24 September 2024
Revised: 14 November 2024
Accepted: 16 November 2024
Published: 19 November 2024

1. Introduction

Europe's Green Deal plan to be the first continent in the world to reach climate neutrality by 2050 [1] and the EU Recovery Plan [2] are encouraging a reduction in GreenHouse Gas (GHG) emissions from the building sector as well as an improvement in energy efficiency. It is intended to reduce 55% of the GHG levels of 1990 by the end of 2030 and 90% by the end of 2040, while also achieving an 11.7% improvement in energy efficiency by 2030. This commitment requires an investment in not only renewable energy but also greater energy efficiency.

In Europe, the building sector is responsible for 36% of total GHG emissions, 70% of which is consumed in heating and cooling [3,4]. Cooling demand is expected to increase significantly by 2050, with a 750% increase in the residential sector and a 275% increase in the commercial sector [5,6]. Due to this tendency, the EU has published various directives and strategies that aim to prevent an increase in GHG such as the directive on energy efficiency (EU/2023/1791) [7] and the EU Strategy on heating and cooling [8]. Among these directives, the concept of district heating (DH) gains significance as it represents a crucial component in energy management for urban environments and a key solution

for mitigating GHG emissions. As a result, DH has experienced numerous scientific and technological advancements in recent years. A more general overview of the advances in district heating worldwide is presented by Werner S. in market, technical, supply, environmental, institutional, and future contexts [9]. For a more European-centralized context, Munćan V. et al. present a detailed view of the state of DH solely in the EU [6]. The maturity of this technology is reflected in the various advances achieved across different generations; the current generations are the 4th generation DH (4GDH) and 5th generation DH (5GDH). Lund H. et al. explain that both generations are not sequential but parallel, and in addition to presenting their differences and similarities, they emphasize that both share the key objective of decarbonization [10]. With this level of implementation, 40 cases of 5GHD in the EU [11], and maturity, the importance of district heating (DH) as part of the solution to decarbonization and the reduction in GHG emissions is clear.

Regarding DH systems aided by geothermal energy, the number of installations has grown in recent years, but it still represents a small percentage compared to other systems, especially due to the high initial investment it commonly requires [12,13]. Taking into account this limitation, many scientific advances and research are focusing on improving the efficiency of this system. This can be achieved by optimizing several parts of the DH system such as the energy supply [14–16], the heat pump [17,18], the control and monitoring of the system [19–21], and the network design [22–24], among others. Sarma U. et al.'s research on enhancing DH efficiency concluded that optimal planning of pipe routes and parameters significantly impacts efficiency [25], a statement that provides a context for this paper. This article aims to show how a change in the type of piping for these geothermal district heating systems can lead to an improvement in thermal efficiency and, consequently, affect the associated consumption. The experiment conducted at a laboratory scale reveals a significant improvement even on a small scale, suggesting that on a larger scale, it would result in considerable improvements in infrastructure cost, feasibility, and overall energy consumption, making DH more efficient and sustainable.

The study of heat transfer in piping systems plays a critical role in the design of efficient energy systems, particularly in industrial applications, where thermal management is essential. Conventional pipe heat exchangers have been widely used due to their simplicity and reliability in transporting thermal energy between two fluids. However, as systems become more complex, new technologies such as coaxial pipes are gaining attention for their potential to enhance heat transfer performance under certain circumstances.

Conventional pipe systems typically consist of two separate pipes, where hot and cold fluids flow independently, allowing for basic heat exchange. While effective, this design is often limited by surface area contact between the fluids, which can reduce the overall efficiency of the heat transfer process [26]. The primary goal in improving heat exchangers is to maximize the contact surface area and reduce thermal resistance, thereby improving the rate of heat exchange. In contrast, coaxial pipes, which involve one pipe, placed inside another, offer a more advanced geometry that can enhance thermal performance by increasing the contact surface between fluids. Studies suggest that the coaxial design allows for better temperature gradients and more efficient heat transfer compared to traditional systems [27]. This design is increasingly used in applications where space is limited and higher thermal performance is required [28].

Delving deeper into the heat transfer process in heat pipes, the most notable innovations in the field include the use of heat accumulators, the application of new technical solutions in the form of pre-insulated pipes, the modification of the heat source, or the integration with other heating networks [29]. Of these solutions, the option of using pre-insulated pipelines stands out, such as using steel pipes with polyurethane foam polyethylene insulation [30]. Other attempts in the context of improving the thermal efficiency of these processes are associated with the introduction of other working fluids with improved thermodynamic properties or the use of other materials in the construction of the distribution systems [31,32]. On the other hand, heat transfer in pipes is addressed by carrying out flow simulations, where different variables and properties of the elements

involved are modified, such as the roughness of the contact surface, flow rate, or outlet pressure, among others [33–35]. All these approaches that are found in the current literature have the common objective of adapting the operating conditions to the optimal performance of the exchange system. However, there are no similar models that refer to the geometry of the heat transfer system in order to increase the overall performance of the heat production facility.

This work presents an innovative coaxial pipe developed in a laboratory as a distribution network in a DH geothermal system. This study also aims to compare the heat transfer performance of these coaxial pipes and the conventional pipe systems under similar conditions. By analyzing their thermal efficiencies, we seek to identify the advantages of the system proposed and provide recommendations for specific applications.

This paper is organized into five sections and four subsections. Section 1, the Introduction, provides the reader with an overview of the context in which this research is framed. In Section 2, information about the methodology followed and the materials required for the experiment to work is given; this section is internally structured with three subsections to ease the reading. The results obtained from the experiment are shown in Section 3, which are discussed in Section 4 with an example of a use case. Finally, Section 5 presents the main conclusion of the paper.

2. Materials and Methods

The experimental methodology consisted of comparing the thermal performance between two pipes designed for geothermal district heating distribution systems. These two pipes, the subject of the comparison, are as follows:

- Simple Pipe: this type of pipe corresponds to the conventional cylindrical pipes implemented in the distribution network of a common geothermal district heating system.
- Coaxial Pipe: This model was designed to be compared against the conventional one. This type of pipe consists of two conventional pipes of different sizes but the same inlet/outlet area, placed concentrically aligned on the same axis.

To perform this comparison, conditions were replicated as closely as possible for both pipes. Consequently, both pipes were manufactured in the same way using 3D printing with the same material.

The print parameters for the specified part are as follows: The selected material for the 3D printing process is ASA (Acrylonitrile Styrene Acrylate), known for its UV resistance and mechanical properties. Table 1 shows ASA's physical, mechanical, and thermal properties.

Table 1. Properties of ASA 3D filament.

Physical Properties				
	Value		**Units**	**Standard**
Density	1.17		g/cm^3	ASTM D792 [36]
Mechanical properties				
	XY value	**ZX value**	**Units**	**Standard**
Tensile Strength	35	15.5	Mpa	ISO 527 [37]
Tensile Modulus	1378	2199.1	Mpa	ISO 527 [37]
Flexural Strength	75.7	39.4	Mpa	ISO 178 [38]
Flexural Modulus	2044.4	1953.8	Mpa	ISO 178 [38]
Elongation at Maximum Load	2.9	0.8	%	ISO 527 [37]
Tensile Elongation at Break	6	0.8	%	ISO 527 [37]
Flexural Elongation at Break	15.3	2.2	%	ISO 178 [38]
Charpy Impact Strength (Unnotched) [1]	50.3	5	kJ/m^2	ISO 179 [39]
Hardness	81.5			ISO 7619-1 [40]

Table 1. *Cont.*

Thermal properties			
	Value	**Units**	**Standard**
Glass Transition Temperature (Tg) [2]	107	°C	ISO 11357 [41]
VICAT B (50 N 50 °C/h) [3]	95	°C	ISO 308 [42]
HDT B (0.45 MPa) [4]	95	°C	ISO 75 [43]

[1] Value that measures a material's resistance to fracture when subjected to a sudden impact. [2] Temperature at which a polymeric material transitions from a rigid state to a more flexible state. [3] Standard test method used to determine the temperature at which a thermoplastic material begins to deform under a specific load. In this case, it is a VICAT test type B with a load of 50 N and a heating rate of 50 °C per hour. [4] Heat Deflection Temperature (HDT) is the temperature at which a plastic material begins to deform under a specified load. In this case, it was tested with the B method with a pressure of 0.45 MPa.

The layer height has been set to 0.2 mm, providing a balance between the surface finish and print time efficiency. A nozzle with a diameter of 0.4 mm is utilized, which is standard for achieving both precision and a reasonable print speed. The infill pattern is concentric, which enhances strength and ensures uniform material distribution. The infill density is set to 100%, ensuring a fully solid structure, which maximizes the mechanical performance of the printed part. Support structures are employed where necessary to ensure overhangs and complex geometries are printed without defects. The estimated print time for the coaxial tube part is 5 h and 20 min, with a total material consumption of 195.51 g. The estimated print time for the simple tube part (Figure 1b) is 4 h and 12 min with a total material consumption of 78.24 g.

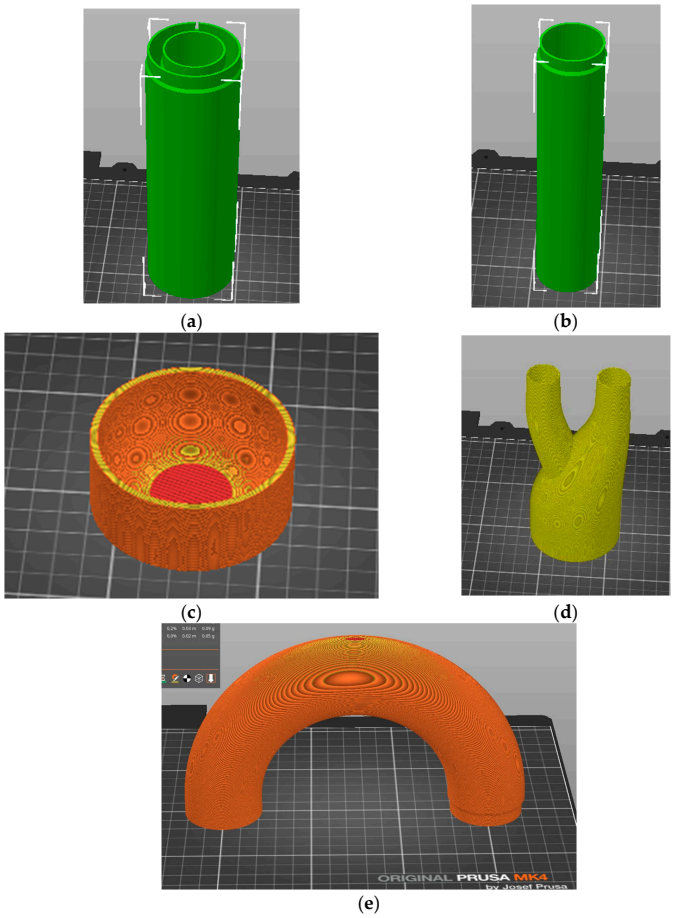

Figure 1. The 3D printed pieces: (**a**) model of the coaxial pipe; (**b**) model of the simple pipe; (**c**) model of the cap-style return piece; (**d**) model of the double-entry piece; (**e**) model of the U-shaped return.

The measurements of the pipes are the result of calculations based on the needs of the optimal area for geothermal district heating in Ávila, Spain [44]. This DH system represents a total demand of 14,078 MWh across 18 buildings. Assuming January's demand as the peak demand (2182.09 MWh), the necessary flow rate must be calculated to meet the daily demand in January (70.39 MWh). Using the following expression, which relates the amount of heat (Q) exchanged by a substance with mass (m), specific heat (C_p), and a known temperature change (ΔT), it can be determined that approximately 12,110 kg of water would be necessary to meet the estimated daily demand.

$$Q = m \cdot C_p \cdot \Delta T \quad (1)$$

where Q is the amount of heat ($2.53 \cdot 10^{11}$ J); m is the mass of the substance; c is the specific heat of the substance (4186 J/g·°C); ΔT is the temperature change (5 °C).

To ensure the development of the test, the following characteristics and conditions of the circulating fluid, pipes, and surroundings in the cases tested have remained under control:

(a) Thermophysical properties of the fluid:
- Density: affects convection behavior.
- Specific heat capacity (Cp): determines how much heat the fluid can absorb or release.
- Thermal conductivity (k): influences the fluid's ability to conduct heat.
- Viscosity: impacts the flow dynamics and, consequently, the convective heat transfer.

(b) Flow conditions:
- Flow velocity: affects the flow regime (laminar or turbulent), which significantly impacts the heat transfer coefficient.
- Flow type (laminar or turbulent): the flow regime can be determined using the Reynolds number.
- Velocity profile: can be fully developed or developing, which influences heat transfer along the pipe.

(c) Temperature conditions:
- Inlet temperature of the fluid: defines the initial thermal energy of the fluid.
- Temperature gradient along the pipe: important for analyzing heat transfer in different sections.
- Temperature distribution of the surrounding environment: should be considered if there is external flow or air around the pipe.

(d) Pipe wall properties:
- Thermal conductivity of the pipe material: affects the heat transfer between the inner and outer fluids.
- Wall thickness: impacts the total thermal resistance of the system.

(e) Pressure:
- Fluid pressure: affects the density and other thermophysical properties.

(f) Boundary conditions:
- Type of heat transfer at the walls: constant temperature, constant heat flux, or un-insulated exterior walls.
- Heat exchange with the environment: forced convection.

All these conditions are crucial to achieving accurate and realistic results in a heat transfer simulation like the one performed in this work.

Therefore, a flow rate of 1513.75 L/h or 0.42 L/s is assumed, which, according to the pressure drop table for PVC pipes, corresponds to a pipe with an internal diameter of 38 mm. To ensure that the conditions on the return of the flow are similar, the areas have been kept constant, resulting in an internal diameter of 54 mm for the outer pipe.

In summary, the base coaxial tube part (Figure 1a) has an interior diameter of the central piece of 38 mm and an interior diameter of the exterior piece of 58.14 mm. Both pieces have a 3 mm thickness to ensure a solid structure. The simple pipe (Figure 1b) has an interior diameter of 38 mm with a 3 mm exterior wall. For both pipes, the base piece length is 20 cm.

Three additional pieces were necessary for the proper functioning of the experiment. The U-shaped return piece (Figure 1e) for the single pipe has an estimated printing time of 3 h and 24 min and a material consumption of 101.88 g. The cap-style return piece (Figure 1c) for the coaxial pipe has an estimated printing time of 1 h and 16 min and a material consumption of 46.80 g. And, lastly, the double-entry piece (Figure 1d) has an estimated printing time of 3 h and 41 min and material consumption of 113.39 g.

Once both pipes are prepared, the experiment involves the recirculation of water under conditions similar to those that a DH distribution system would operate under.

The following sections describe the components used to replicate the DH distribution system as well as the methodology employed for conducting the experiment.

2.1. Components Used

To replicate the DH distribution system on a laboratory scale, the following components have been used:

- A boost pump. The pump used 3 W of power. This pump allowed the circulation of the fluid in a constant volume of flow of 6.91 L/h. A clear tube of 2.20 m was used to feed the pump onto the pipeline.
- A 3D printer. Any filament 3D printer capable of high thermal resistance filaments can be used. The print size is not limiting; more parts can be produced. In this study, the Original PRUSA MK4 3D Printer model has been used (Figure 2a).
- A 3D filament. As mentioned in Section 2, the material used for 3D printing was ASA filament. ASA filament properties are presented in Table 1.
- Assembly material. Waterproof tape for pipe joints to ensure no critical leaks among the pipelines.
- Water. The fluid used for the recirculation is water with no special specification.
- A water tank. A tank to set the water for the experiment is needed to have enough flow through the pipeline during the recirculation. The measurements of the tank used were 0.60L $\times$ 0.20W $\times$ 0.45H m.
- A resistant heater. The heater was set onto the water tank to establish and maintain a certain work temperature. The resistance range falls within 10 °C to 100 °C.
- Thermocouples. Inlet and outlet temperatures of the fluid were controlled by thermocouples connected to a measuring device (thermometer). The inlet temperature was taken by measuring the temperature of the water tank, and the outlet temperature was measured at the end of the pipeline. In this experiment, the thermocouples used were constituted by chrome and aluminum alloys (type K), had an accuracy of $\pm$0.01 K, and were calibrated according to the International Law ASTM E220 [45].
- A thermometer. As a measuring device, a multichannel digital contact thermometer model PCE-T390 was used. This model allows for a measuring range for K-type thermocouples from $-$100 to +1370 °C.
- Ice. A tray of 0.39L $\times$ 0.39W $\times$ 0.05H m was filled with ice to help increase the gradient between the inlet and outlet.
- A flowmeter: The flowmeter employed was the model PCE-TDS-200 from the PCE Instruments company (Albacete, Spain), which has a measuring range of 32 m/s and a resolution of 0.001 m/s, for diameters exceeding 50 mm, and an accuracy of +1.5% of the value (v > 3 m/s). The device is suitable for use in a fluid temperature range from $-$30 °C to +160 °C. The pipe materials can be diverse, such as polyethylene and polyvinyl chloride (PVC). It can be used in a wide range of media, like water, oil, diesel ethane, and others [46].

(**a**) (**b**)

Figure 2. Resources used for the experiment: (**a**) professional 3D printer used for this test; (**b**) sample of the test pipes. The simple pipe can be seen on the right side, and the studied pipe, the main subject of comparison, is placed on the left.

Using the 3D printer with the ASA filament, the pipeline can be printed. For this experiment, a total of 1.2 m of pipeline for both types were printed. Figure 3 shows the schematic model of the coaxial pipeline, whereas Figure 4 shows the schematic model of both pipelines with measurements for easy replicability.

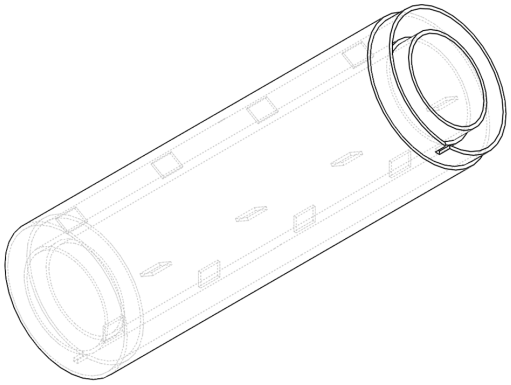

Figure 3. Model of the coaxial pipeline (patented).

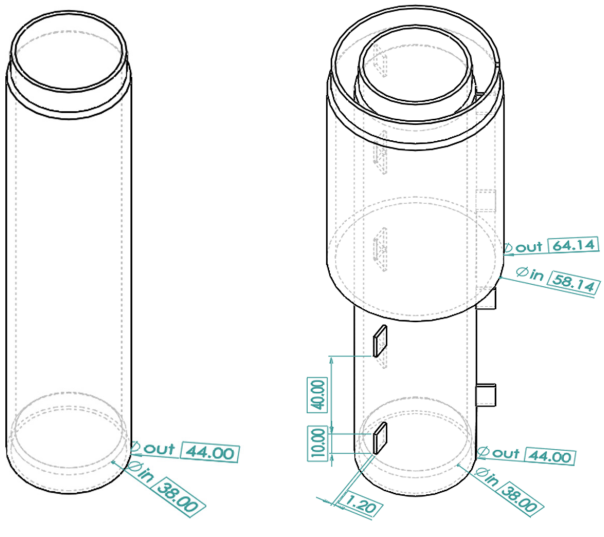

(**a**) (**b**)

Figure 4. Model of the simple pipeline (**a**) and coaxial pipeline (**b**) with measurements for replicability.

2.2. Theoretical Base

In district heating systems, energy efficiency and heat recovery are key aspects for optimizing overall system performance [47,48]. The comparison between coaxial and conventional pipelines focuses on how these structures can influence heat recovery and thermal efficiency in the boiler room. When designing heat exchangers, in this case involving coaxial and conventional tubes, several initial conditions must be kept in mind. The following known conditions are critical for guiding both the design and subsequent calculations:

- Fluid properties: the thermal conductivity, specific heat, viscosity, and density of the working fluid often vary with temperature, requiring the use of average or temperature-dependent values during the design process.
- Flow rates: The mass flow rate of the fluids plays a significant role in the heat transfer process. The flow can be either laminar or turbulent, depending on the Reynolds number, and this greatly influences the heat transfer coefficients and pressure drops within the system.
- Inlet and outlet temperatures: The inlet temperatures of both the hot and cold fluids, along with their desired outlet temperatures are the key to the performance comparison. The difference in temperature between the fluids at different points affects the overall heat transfer rate and is the measure selected to compare the different systems.
- Pressure conditions: In some cases, the system must also meet certain pressure requirements. These constraints can impact the selection of pipe materials and dimensions, particularly in high-pressure environments where failure could lead to safety concerns. In this study, this is not the case, and the only measure is to maintain the same pressure conditions.
- Geometry constraints: Space limitations and installation requirements also influence the design. For example, coaxial pipes are often chosen for their compact geometry, making them suitable for applications where conventional tube bundles would take up too much space

Apart from the initial conditions above, several other considerations have been taken into account in the design phase:

- Maximizing heat transfer efficiency: The goal is to maximize the amount of heat transferred between fluids for a given size and configuration of the system. Coaxial pipes, with their increased surface area contact, are often chosen for applications requiring high thermal efficiency.
- Minimizing pressure losses: Pressure losses lead to higher pumping costs and reduced system performance. Designers aim to minimize these losses while maintaining adequate fluid velocity to support effective heat transfer.
- Material and cost efficiency: The selection of materials is influenced by both thermal conductivity and cost considerations. Engineers must balance performance requirements with material costs, while also considering the durability of the chosen materials.

2.2.1. Heat Recovery in the Boiler Room

Heat recovery is the process by which residual heat from the heating system is captured and reused, thus improving energy efficiency and reducing heat loss. In a district heating system, this process can be optimized through the use of different pipeline designs [49,50].

2.2.2. Conventional Pipelines

In a conventional system, the supply and return pipes are separate, meaning the residual heat from the return water is not directly used to heat the supply water. The heat loss in these pipes can be described by Equation (2), which takes into account the heat loss by conduction, convection, and radiation [51]:

$$Q_{loss} = U \cdot A \cdot \Delta T \quad (2)$$

where Q_{loss} is the amount of heat lost; U is the overall heat transfer coefficient that includes the inside and outside convective heat transfer coefficient, the thermal conductivity of the material, the radiative heat transfer coefficient, and the thickness of the pipe; A is the surface area of the pipe; and ΔT is the temperature difference between the inlet and outlet fluids.

In this sense, heat is transferred by convection from the inlet fluid to the wall of the pipe, by conduction through the pipe wall, and then by convection from the pipe wall to the outlet fluid. It must be clarified that, considering the orders of magnitude of the temperatures on the pipe surface of the analyzed study case, the loss due to radiation will not be included in the corresponding calculations.

2.2.3. Coaxial Pipelines

Coaxial pipelines integrate the supply and return lines within a single structure. The coaxial design allows for better heat recovery because the return water circulates around the supply water, capturing some of the heat that would otherwise be lost. The global heat transfer in a coaxial pipe can be modeled using the same Equation (2), but the constructive peculiarities of this system must be taken into account. Thus, in this case, heat is transferred by convection from the inlet fluid to the wall of the pipe, by conduction through the inlet pipe wall, by convection from the pipe wall to the outlet fluid, again by conduction through the outlet pipe wall, and finally, by convection from the outlet pipe to the external fluid (radiation is considered in the same way as in the conventional pipe case) [52].

2.2.4. Heat Transfer Evaluation

As stated before, heat transfer in a piping system such as those presented here is subjected to heat losses from the internal fluid by thermal conduction (through the pipe wall) as well as by convection to the outside air. Thus, the conduction and convection heat calculated in a cylindrical pipe are shown in Equations (3) and (4).

$$q = \frac{2\pi k}{2.3log\left(\frac{D_2}{D_1}\right)}(T_1 - T_2) \tag{3}$$

$$q = h\pi D_2(T_2 - T_a) \tag{4}$$

where k is the thermal conductivity of the pipe material in W/m·K, h is the convective coefficient in W/m^{2}K, D_2 and D_1 are the external and internal pipe diameters (m), and T_1, T_2, and T_a are the internal and external pipe temperature and the ambient temperature, respectively, in K.

Combining the previous equations in a single expression that reflects the global heat flow throughout the entire transfer area, the final expression, Equation (5), is as follows:

$$q = \frac{\pi(T_1 - T_a)}{\left(\frac{2.3}{2k}log\frac{D_2}{D_1} + \frac{1}{hD_2}\right)} \tag{5}$$

In the case of estimating the heat loss in the case of the conventional system, *Ta* would correspond to the conditions of the fluid outside the piping system, while the calculation of this loss in the coaxial pipe (heat recovery in the return fluid) would take as *Ta* the temperature of the fluid circulating through the outer section.

2.2.5. Heat Recovery Efficiency

The heat recovery efficiency (r_e) in a coaxial pipe can be defined as the ratio of the recovered heat to the total heat available in the return water:

$$r_e = \frac{Q_{recovered}}{Q_{return}} \tag{6}$$

where Q_{return} is the total heat of the return water, given by the following:

$$Q_{return} = \dot{m} C_p (T_{return} - T_{ambient}) \quad (7)$$

where $\dot{m}$ is the mass flow rate of the return water; C_p is the specific heat capacity of water; T_{return} is the temperature of the return water; and $T_{ambient}$ is the ambient temperature (25 °C).

2.2.6. Efficiency Comparison

To compare the efficiencies between coaxial and conventional pipelines, the efficiency of each system can be calculated, and the differences in terms of heat recovery and energy losses can be analyzed.

For a conventional pipe,

$$r_e = 1 - \frac{Q_{loss}}{Q_{total}} \quad (8)$$

where Q_{loss} is the amount of heat lost, and Q_{total} is the total heat supplied to the system.

For a coaxial pipe,

$$r_e = 1 - \frac{Q_{loss} - Q_{recovered}}{Q_{total}} \quad (9)$$

where Q_{loss} is the amount of heat lost; $Q_{recovered}$ is the recovered heat; and Q_{total} is the total heat supplied to the system.

These equations show how the coaxial design can potentially improve heat recovery efficiency compared to conventional pipes.

2.3. Methodology

To conduct the laboratory experiment, the setup schema presented in Figure 5 must be followed. The first step is filling the water tank to the necessary level that covers the working limit of the heater. Once filled, the heater can be placed and started. On the other hand, the pipe pieces must be assembled (Figure 6). The flow inlet piece of the pipeline must be connected to the boost pump tube. For the proper flow of water, it is necessary that the pipe is positioned in such a way that the flow outlet piece is aligned with the water tank. In this way, continuous water flow is ensured.

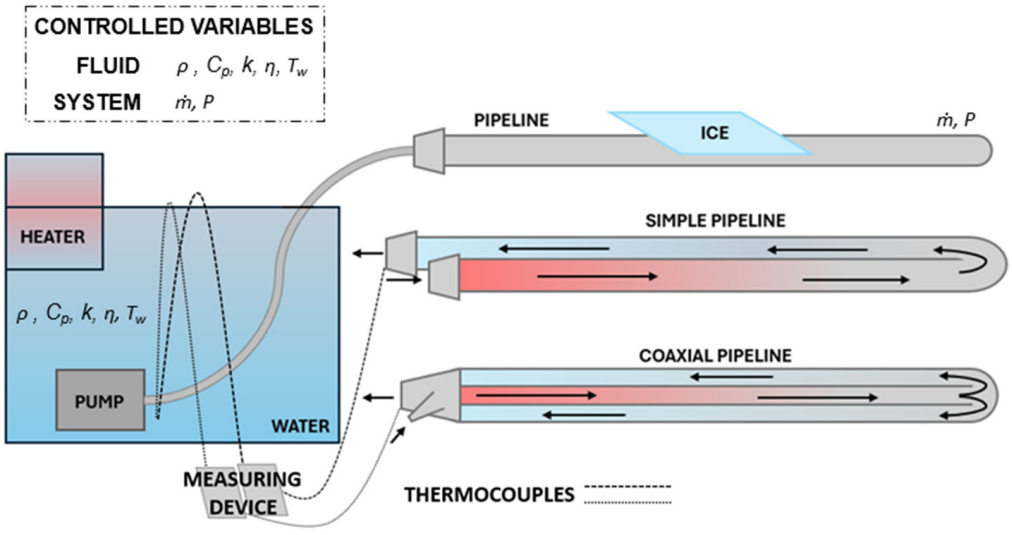

Figure 5. Experiment setup schema.

When the pipeline is set, and the water has reached the desired temperature, the boost pump can be started and placed inside the water tank. Figure 7 shows the experiment with the boost pump placed. It might be considered that, given that the water tank is not

sealed, evaporation due to temperature may occur, and it may be necessary to add water to maintain the level.

Figure 6. Both pipelines assembled.

Figure 7. A sample of the experiment setup with the pipe and the water circulation pump.

Since the length of the pipe has been reduced to 1.2 m for a laboratory scale, ice has been used on the pipe to ensure a sufficient thermal gradient for measurement. This ice simulates the heat loss in the distribution network at the laboratory level.

Once the experiment is set up and running, with a continuous flow of hot water, the measurement equipment should be prepared. As presented previously, a thermocouple will be used to continuously control and record the temperature of the inlet and outlet. For the inlet temperature, the thermocouple was placed inside the water tank, near the boost pump. The outlet temperature was measured by placing the thermocouple at the end of the pipeline, just when the water was released into the water tank (Figure 5 for reference of placement). Once the water tank temperature was stable (71.5 $\pm$ 1.5 °C), both inlet and outlet temperatures began to be registered.

3. Results

3.1. Fluid Temperature Evolution

The temperature measurements of the experiment are presented in the following graphs. Both pipelines, simple and coaxial, had their temperature measurements taken every 2 s, which resulted in 600 measurements in 20 min.

The initial presentation of the results is based on the original measurements obtained from the thermocouple readings. Firstly, the results of the inlet and outlet temperatures of the pipe were obtained for both experiments (coaxial and simple pipelines). Once recorded, the temperature difference between the inlet and outlet was calculated, resulting in the temperature gradient. This gradient has been represented on the Y-axis, while the measurement number is represented on the X-axis. These graphs serve to broadly observe the stability of temperature variation and discern the overall trend. Thus, Figure 8, for the simple pipeline, and Figure 9, for the coaxial pipeline, show the temperature gradients for each measure taken.

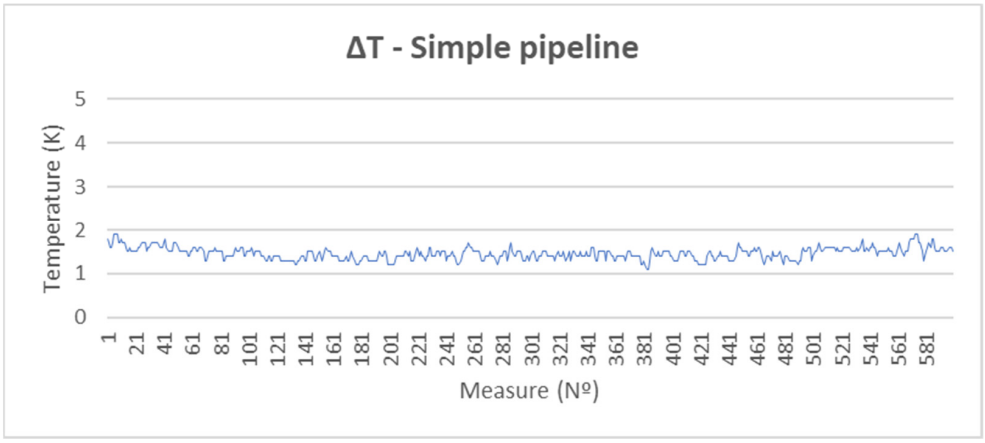

Figure 8. An overview of the temperature gradient from the measures taken (simple pipeline).

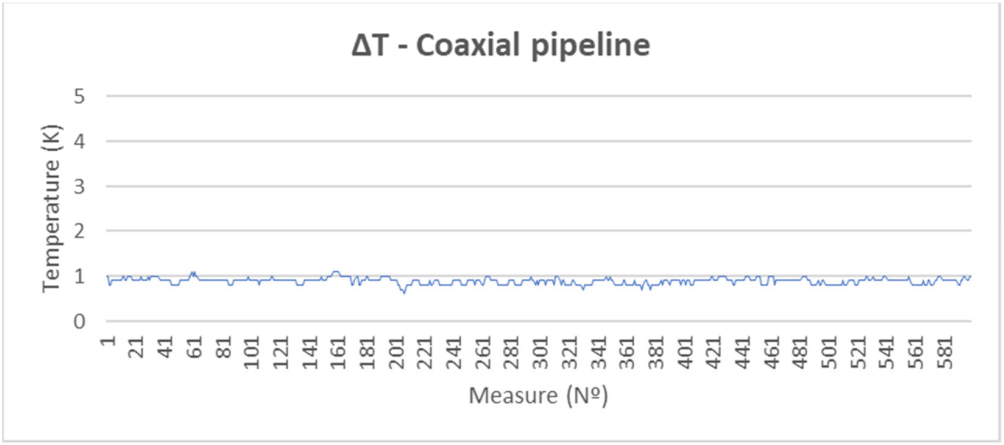

Figure 9. An overview of the temperature gradient from the measures taken (coaxial pipeline).

In Figures 10 and 11, the same concept is presented but with an adjustment on the *Y*-axis to facilitate detailed viewing. In the previous figures, the *Y*-axis covered a range of up to 5 degrees of temperature difference. However, after the initial review of the data, this range can be narrowed down to 2 degrees for the single pipe and 1.2 degrees for the coaxial pipe. This change allows for a better visualization of the results, as a total of 600 measurements are shown. Additionally, these graphs have been presented with a line depicting the average of the results (orange dotted line). The addition of this line visually indicates the average value around which the measurements cluster. A preliminary observation confirms that the coaxial pipe shows lower values, which aligns with the design that enhances heat transfer from the inlet to the outer jacket of the outlet. However, the numerical details are presented in Table 2.

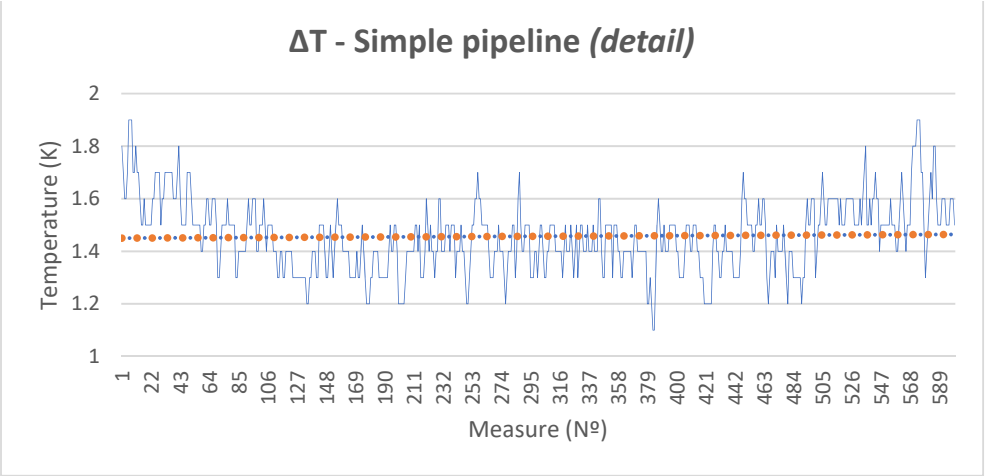

Figure 10. Results of the temperature gradient from the measures taken in an adjusted *Y*-axis (simple pipeline).

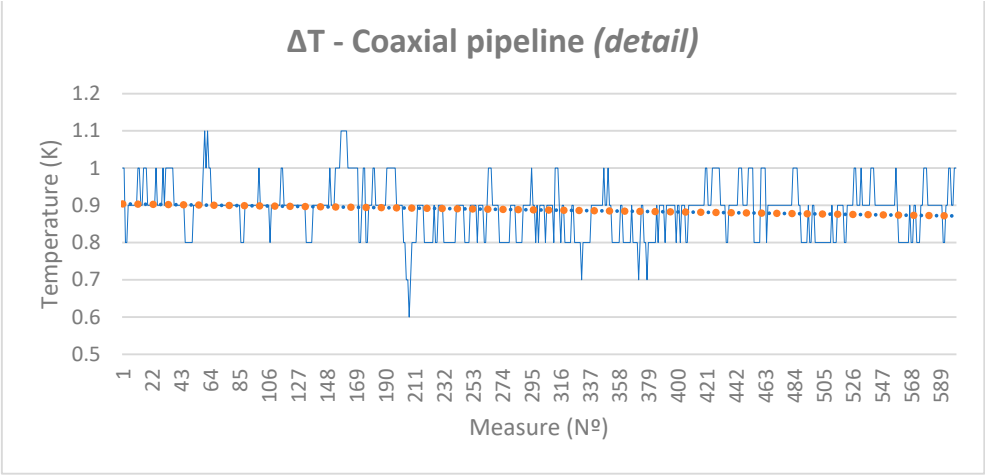

Figure 11. Results of the temperature gradient from the measures taken in an adjusted *Y*-axis (coaxial pipeline).

Table 2. Data comparison between the simple pipeline and coaxial pipeline (K).

Pipeline Type	Mean	Median	Mode	Max. Value	Min. Value
Simple	1.45	1.50	1.50	1.90	1.10
Coaxial	0.88	0.90	0.90	1.10	0.60

In Table 2, the most representative statistical measures of the central tendency that describe the distribution of the sample set are presented. As can be observed, the simple pipeline shows higher values compared to the coaxial pipeline, which is an expected result since the coaxial pipe promotes heat transfer along its length, allowing for a smaller temperature loss between the inlet and outlet. It should be noted that these measurements are subject to the intrinsic error of the thermocouple and meter calibration (±0.01 K) as well as random errors such as unpredictable variations, which may include thermocouple movement caused by water flow, among other factors. Therefore, as a mitigation measure, the measuring instrument has been calibrated according to the International Law of the "Standard Test Method for Calibration of Thermocouples By Comparison Techniques" ASTM E220 [45], as mentioned in 2.1 Components used. Moreover, multiple measurements have been conducted, which are visible in the graphs.

Given that the experiment involves the analysis of measurement data, the standard deviation (SD) (Equation (10)) has been calculated to assess the dispersion of the values around the mean of the dataset.

$$\sigma = \sqrt{\frac{1}{N-1}\sum_{i=1}^{N}(x_i - \overline{x})^2} \quad (10)$$

where σ is the SD; N is the number of data points in the population; x_i represents each data point; and $\overline{x}$ is the population mean.

Additionally, the confidence interval (CI) has been calculated using the following equation (Equation (11)). A confidence interval is understood as the range of values used to estimate the true parameter of a population based on sample data. The confidence levels used are 90%, 95%, and 99%.

$$CI = \overline{x} \pm z_{\alpha/2} \cdot \frac{\sigma}{\sqrt{N}} \quad (11)$$

where CI is the confidence interval; $\overline{x}$ is the population mean; $Z_{\alpha/2}$ is the critical value corresponding to the desired confidence level (±1.645 for 90%; ±1.96 for 95%; ±2.576 for 99%); σ is the DS; and N is the number of data points in the population.

The standard deviation values and the confidence interval are presented in Table 3.

Table 3. Statistical data comparison between the simple pipeline and coaxial pipeline.

Pipeline Type	Dif. Max.	Dif. Min.	SD	CI 99%	CI 95%	CI 90%
Simple	0.45	−0.35	0.135	±0.0142	±0.0108	±0.0091
Coaxial	0.22	−0.28	0.071	±0.0075	±0.0057	±0.0048

As can be observed, the standard deviation is low, indicating that the measurements are quite clustered around the mean. The confidence intervals for the three confidence levels are considered appropriate, as such narrow intervals are very precise. However, as seen from the difference between the maximum and minimum values of both pipes (calculated as the mean value minus the peak value), there is significant variation, suggesting the presence of some outlier values due to indirect measurement errors. In order to minimize this error, a modification of the previously presented data has been made. This modification involves grouping the measurements into 1 min intervals, with the value assigned to each interval being the average of all the values recorded during that minute. The new values are presented in Figures 12 and 13. Therefore, these graphs represent the temperature gradient over time in minutes with the averaged data from the measurements taken each minute.

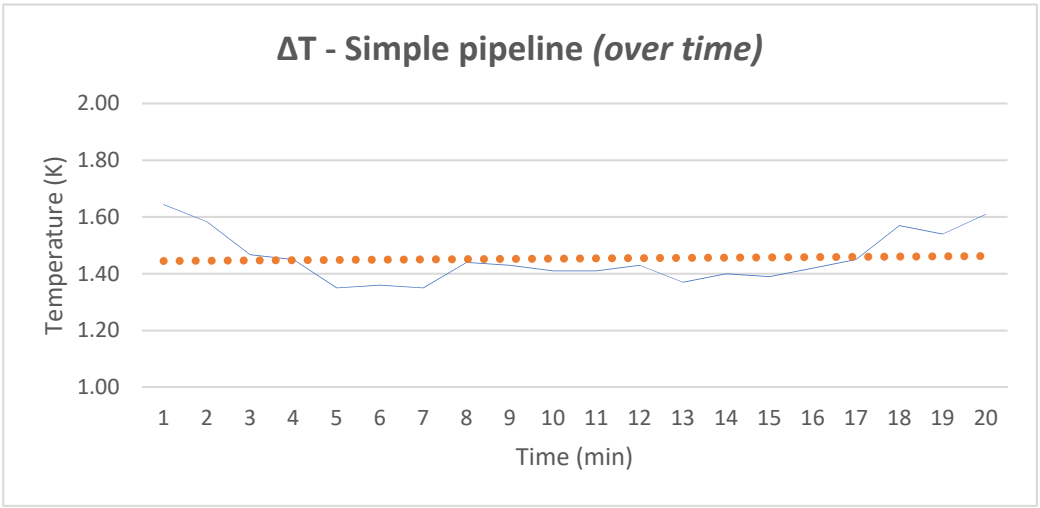

Figure 12. Results of the temperature gradient from the measures taken based on 1 min time intervals (simple pipeline).

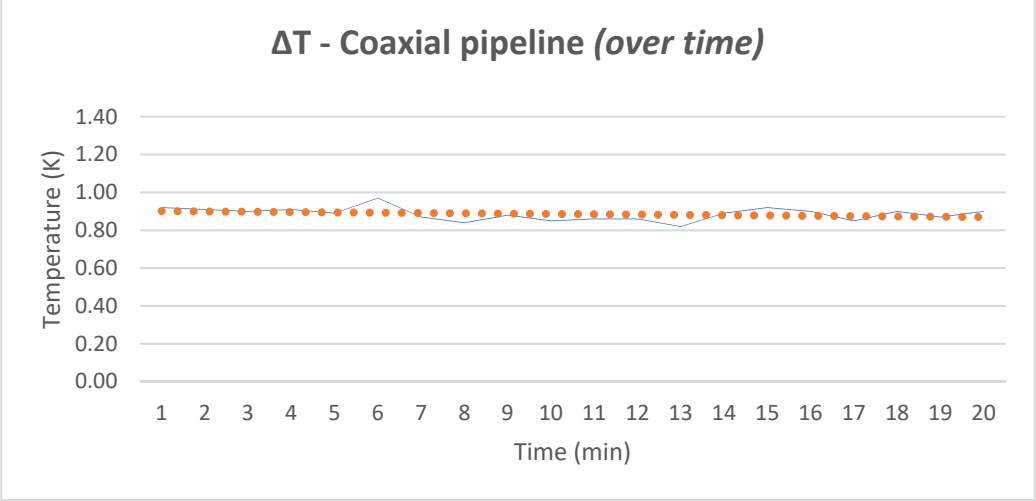

Figure 13. Results of the temperature gradient from the measures taken based on 1 min time intervals (coaxial pipeline).

With the adjustment completed, it is evident that there is a very noticeable stabilization period, especially in the single pipeline. For an accurate evaluation of the results, the first and last 3 min of the measurement have been excluded, and the new representations of this approach can be seen in Figure 14 for the simple pipeline case and in Figure 15 for the coaxial pipeline case. Additionally, Figure 16 shows both pipeline results for an easy comparison.

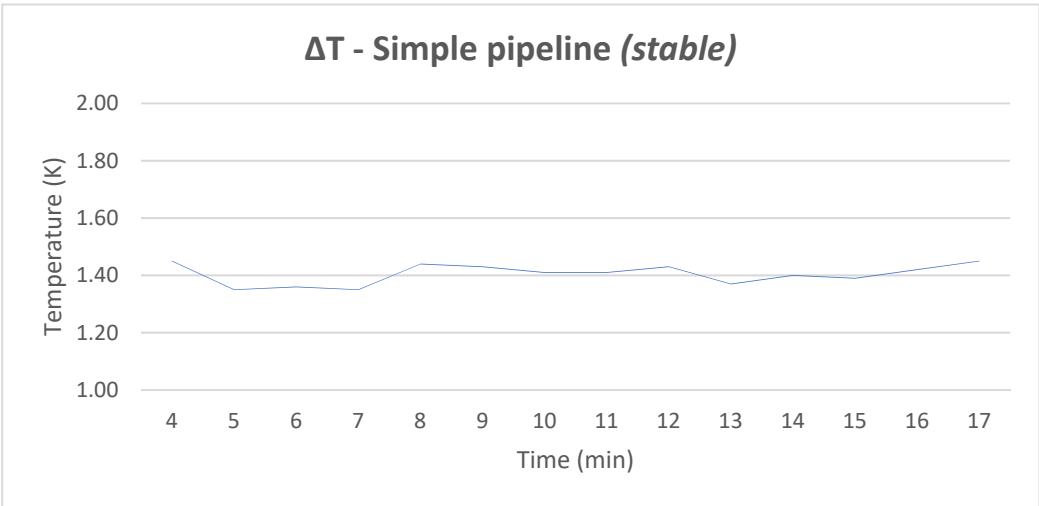

Figure 14. Results of the temperature gradient from the measures taken based on time without the stabilization (simple pipeline).

With these new adjustments, the values presented in Table 2 have changed. Table 4 shows the new values to take into consideration.

Table 4. Data comparison between the simple pipeline and coaxial pipeline after adjustments (K).

Pipeline Type	Mean	Median	Mode	Max. Value	Min. Value
Simple	1.40	1.41	1.45	1.45	1.35
Coaxial	0.88	0.88	0.89	0.97	0.82
Difference	−0.52				
Decrease	37.14%				

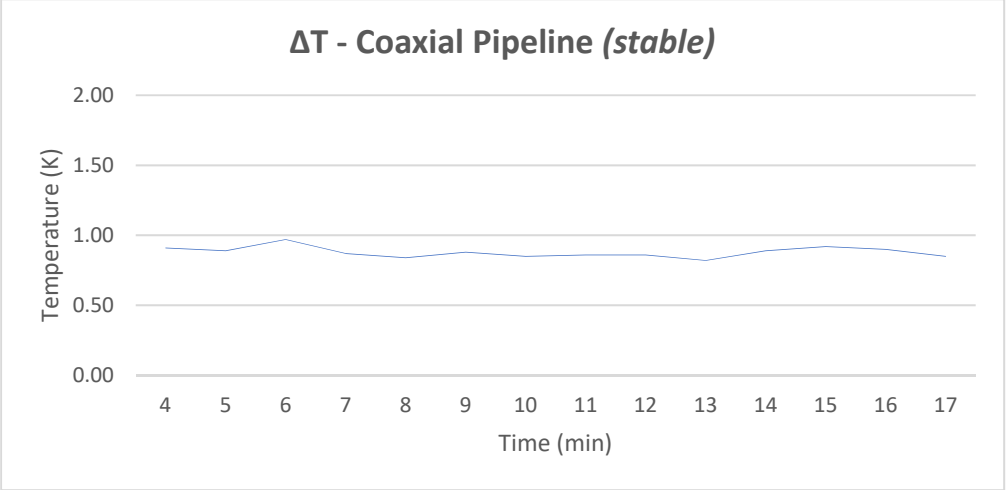

Figure 15. Results of the temperature gradient from the measures taken based on time without the stabilization (coaxial pipeline).

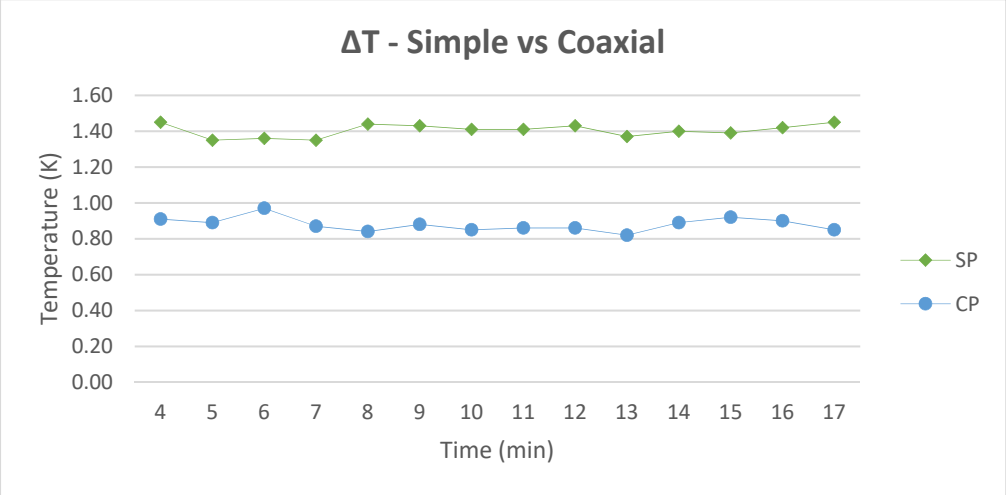

Figure 16. Comparison between the temperature gradients of the simple pipeline (SP) and coaxial pipeline (CP).

This difference between models results in a **decrease of 37.14%**.

Following Equations (10) and (11), the SD and CI have been recalculated with the new adjusted values. Table 5 shows the results obtained.

Table 5. Statistical data comparison between the simple pipeline and coaxial pipeline after adjustments.

Pipeline Type	Dif. Max.	Dif. Min.	SD	CI 99%	CI 95%	CI 90%
Simple	0.05	−0.05	0.034	±0.0179	±0.0235	±0.0150
Coaxial	0.09	−0.06	0.037	±0.0193	±0.0254	±0.0162

As can be observed with the new adjustment, the difference between the maximum and minimum values of both pipes is now under ±0.1 K compared to the ±0.5 K of the original values (Table 3). This means that the occasional measurement errors have been smoothed out, and the adjusted values can be considered more precise and clustered around the mean. This last point can be verified with the new values obtained from the calculation of the standard deviation, where both pipe models show lower values, especially in the single pipe after adjusting for the exclusion of stabilization data. Regarding the confidence

interval, a minimal variation can be observed due to the reduction in the number of samples considered for the calculation, 600 measures against 14 for the adjusted model.

3.2. Heat Transfer

In order to thoroughly evaluate the difference in heat exchange between the tested systems, this section presents an analysis of the heat losses in each of the pipes developed under the conditions of the laboratory experiment. It is worth mentioning that, in the case of the coaxial system, this heat transfer from the internal fluid is considered a contribution to the fluid circulating through the external envelope.

Applying Equations (3)–(5), the heat loss and the heat recovered can be estimated. All the values of these equations are known, except for the convective coefficient, which must be calculated for the conditions of the tests. In the case of the simple pipe, this would be the convective coefficient of the outside air, and in the coaxial pipe, it would correspond to the convective coefficient of the fluid circulating in the outside branch.

To determine the convective heat transfer coefficient (h) of both fluids, parameters about the flow behavior, such as the Nusselt, Reynolds, or Prandtl number as well as the flow rate, density, dynamic viscosity, and thermal conductivity, have been considered. From the calculation of these parameters, the results of the convective coefficient and the heat transfer for both systems are presented in Table 6.

Table 6. Convective coefficient for the air (h_a) (in the case of the simple pipe), the water (h_w) (for the coaxial pipe), and the heat transfer per unit of pipe length (q).

Pipeline Type	h_a/h_w (W/m^{2}K)	q (W/m)
Simple	66.25	279.64
Coaxial	2374	14.28

As derived from the above, the selection of the coaxial geometry for heat distribution reduces the heat loss in the internal distribution pipe, achieving in turn that this loss becomes useful in the return of the fluid to the generation plant. The heat loss of the simple pipe with the exterior is similar to that which will occur on the exterior of the coaxial pipe in the case of not selecting the correct insulation for them.

4. Discussion

Beyond the above and in order to evaluate how the design of the coaxial system would affect a geothermal district heat network, this section presents a comparison of this design with respect to the conventional one in a specific case study. For this, the network shown in Figure 17 is selected, which includes three large buildings located in the region of Salamanca, Spain (Figure 18).

To carry out the planned evaluation, the following Table 7 includes information on the construction date of the buildings and their associated energy demand.

Table 7. Construction date and energy demand per building selected.

Building	Construction Date	Energy Demand (MWh)
1	1980	5984.18
2	2007	5099.45
3	1999	10,098.50
Total energy demand (MWh)		**21,182.12**

In addition, Table 8 shows the principal parameters considered for the calculation of the geothermal system.

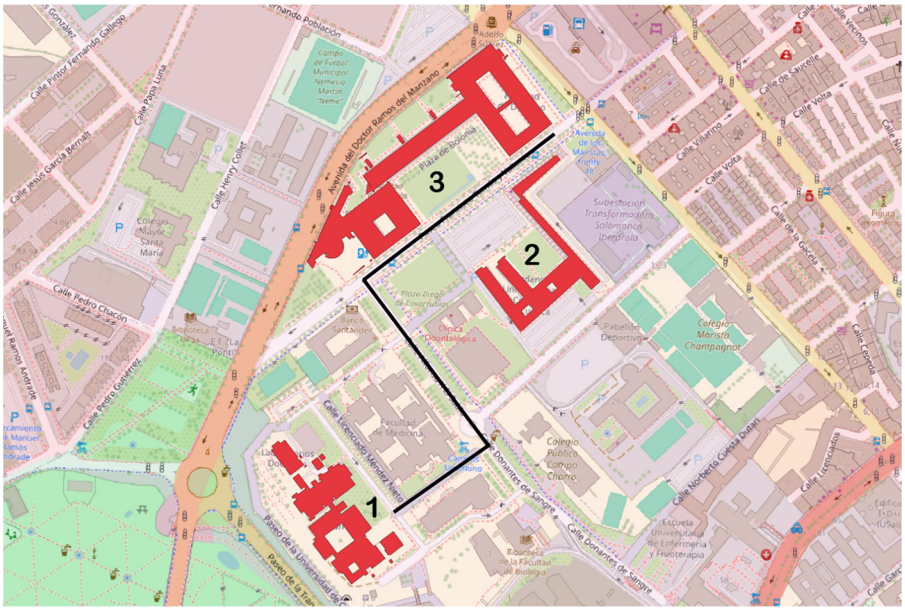

Figure 17. Buildings integrating the geothermal district heating here considered.

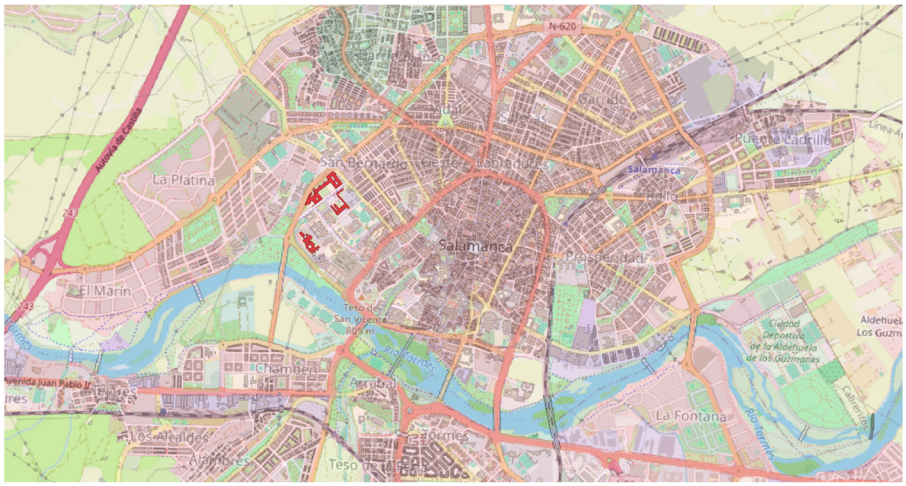

Figure 18. The location of the buildings selected in Salamanca, Spain.

Table 8. Design factors considered for the geothermal system selected.

Design Factors—Principal Parameters	
Thermal conductivity of the terrain	1.6 W/mK
Working fluid	67% Water—33% Monopropyleneglycol
Volumetric capacity	2.4 MJ/(m^3·K)
Geothermal heat flow	0.09 W/m^2
Heat exchangers	Double-U polyethylene 32 mm
Filler thermal conductivity	1.47 W/mK

It is convenient to clarify that all the previous information is the same for the two scenarios (coaxial and simple), but, given the difference in ranges in the operating temperatures (inlet and outlet), there is a difference in the performance that involves the heat pump taking over the generation of the same amount of requested energy. Typically, a geothermal district heating system with a traditional distribution system has an associated thermal jump of about 27.5 °C [47]. This type of installation with high-power heat pumps usually operates with a Coefficient of Performance (COP) of around 3.3 for a thermal jump, as indicated [53].

Taking this into account, this section aims to analyze how the replacement of the simple distribution system affects the coaxial one based on the variation in the thermal jump (as has been experimentally seen to be lower in the coaxial design). To do this, the percentage of thermal jump reduction obtained in the laboratory (Table 4) is considered to be one of the maximum possible, and the benefit obtained from this compared to other scenarios with a smaller difference in thermal range will be observed. Based on previous studies, it is known that for a temperature increase of 10 °C, a geothermal heat pump COP of six is associated, while for an increase of 20 °C, the COP of the system would be four [50]. Considering all the previous information, the relationship between the thermal jump in the distribution branch fluid and the COP performance of the high-power heat pump has been estimated. Thus, the calculated values for each of the assumptions related to the different thermal decreases are presented in Table 9. Table 9 also presents the estimated economic and environmental benefits derived from the reduction in the thermal jump in this kind of geothermal installation. It is important to notice that, in the conventional system, inlet and outlet temperatures have been estimated as 65 °C and 40 °C, respectively.

Table 9. An evaluation of the working parameters associated with each scenario of thermal decrease and economic and environmental annual factors.

Thermal Difference Decrease (%)	Thermal Difference (°C)	COP	Heat Pump Power (kW)	Heat Pump Energy Demand (MWh)	Saved Energy (MWh)	Economic Savings (€)	CO_2 Emissions Reduced(kg)
37	15.75	4.70	1877.66	4506.38	1911.80	167,148.67	497,068.00
30	17.50	4.38	2014.84	4835.67	1582.51	138,358.85	411,452.60
20	20.00	4.00	2206.25	5295.00	1123.18	98,199.63	292,026.80
10	22.5	3.69	2391.60	5739.84	684.34	59,831.85	177,928.40
5	23.75	3.57	2471.99	5932.77	485.41	42,439.40	126,206.60
0 (simple design)	25.00	3.30 *	2674.24	6418.18	--	--	--

* According to the curve fit, the tabulated value is 3.46, but 3.3 is used since a real reference value is available.

Since the use case is located in Spain, the value of the kWh and the kg of CO_2 per electric kWh are based on the Spanish market. In 2023, the emission factor was 0.260 $kgCO_2$/kWh for the electric mix [54]. As for the price, the mean market price for 2023 was 87.43€/MWh [55].

From the above Table 9, it can be deduced that significant energy saving occurs the greater the decrease in thermal difference. Analyzing these scenarios with a view to a useful life period of 25 years, the amount of energy that can be saved for this district heating system is quite significant. This variation is shown in the following graph of Figure 19, where differences of approximately 40,000 MWh can be seen between the most extreme cases.

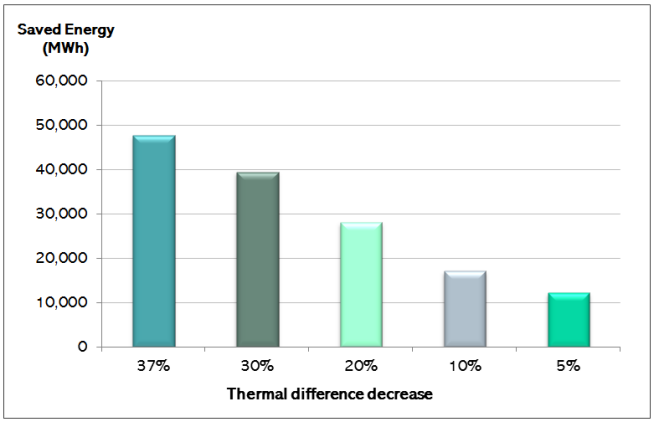

Figure 19. The saved energy associated with each thermal difference decreases for a useful life period of 25 years.

5. Conclusions

The present study aims to present and evaluate a novel experimental distribution network as an improvement to geothermal district heating systems. Currently, the main advances for these systems, as stated in Section 1, are applied to the design, the heat pumps, supervising and monitoring, or pipelines. It is in this last area that this study applies an improvement by proposing a new type of distribution pipeline. In this specific case, it is proposed to replace the traditional single-pipe system with a novel coaxial pipe system.

For the study of this comparison at a laboratory scale, certain simplifications have been made, and the following points should be highlighted:

- Both pipes have been 3D printed with the same material, under the same conditions, and have the same length in meters.
- To simulate at a laboratory scale, the gradient generated by the use of the system in distribution and the same ambient and cooling conditions have been applied in both studies.
- The same conditions have been maintained for the measurement of both pipes.

Under these circumstances, a 37% improvement (37.14%) in the thermal exchange has been achieved with the new coaxial model. This percentage is obtained from the average comparison between the inlet and outlet temperatures of both systems, showing that at a laboratory scale, a significant improvement in the thermal exchange is achieved. Furthermore, calculations on both systems show that the heat loss associated with the coaxial system from the internal fluid represents an additional energy contribution to the fluid that returns to the generation plant, thus demonstrating that the proposed distribution system represents an improvement in the overall performance of the installation.

In addition, and although it is very challenging to apply this value to a real-world case (as laboratory conditions are considered ideal), to validate the advantages of this change in the pipe type, a simple geothermal district heating system has been modeled for the city of Salamanca, Spain. The technical specifications, system design, and data used are detailed in Section 4.

Based on the results obtained, different scenarios have been evaluated, where the most optimistic scenario reflects the 37% improvement observed in the laboratory, while the most pessimistic scenario ranges from no change to a 5% improvement. Various percentages between these two positions have been assessed, as shown in Table 5. In summary, in the most pessimistic scenario of a 5% improvement, the annual economic savings based on energy savings amount to approximately €42,000, with a related reduction in emissions of about 126,000 kg of CO_2. In the best-case scenario, these figures increase to €167,000 in savings and a reduction of 497,068 kg of CO_2. Therefore, not only is the economic and energy savings of significant value but, in terms of emissions reduction (kg of CO_2), it represents a considerable improvement.

In future research, the coaxial pipe model will be tested with other types of materials and different parameters according to the needs of real cases, including variations in diameter, increased length, and even different inflow and outflow rates. To this end, various scenarios will be studied to facilitate new data collection for a reassessment of the obtained results.

6. Patents

The coaxial pipe is under patent protection "Tubería Coaxial para sistemas de recirculación" under University of Salamanca.

Author Contributions: Conceptualization, C.S.B., I.M.N. and N.N.-V.; methodology, C.S.B., I.M.N., M.Á.M.-G., V.P.F. and N.N.-V.; software, E.G.-G.; validation, C.S.B., I.M.N. and N.N.-V.; C.S.B., I.M.N. and N.N.-V.; investigation, C.S.B., I.M.N., E.G.-G., M.Á.M.-G., V.P.F. and N.N.-V.; resources, D.G.-A. and A.F.M.; data curation, C.S.B., I.M.N. and N.N.-V.; writing—original draft preparation, C.S.B., I.M.N. and N.N.-V.; writing—review and editing, M.Á.M.-G., D.G.-A. and V.P.F.; visualization, V.P.F.;

supervision, C.S.B. and A.F.M.; project administration, C.S.B.; funding acquisition, D.G.-A., and A.F.M. All authors have read and agreed to the published version of the manuscript.

Funding: This research received no external funding.

Institutional Review Board Statement: Not applicable.

Informed Consent Statement: Not applicable.

Data Availability Statement: Data are contained within the article.

Acknowledgments: This research was supported by the research projects support program, co-financed by the European Regional Development Fund (ERDF), under the order of the Ministry of Education from Castilla y León. (project ref.: SA102P20) and has been carried out within the framework of the main research "Development and integration of a new district heating system using low-energy geothermal energy (GEO-DISTRICT 3.0)" and under the project GEO-ROAD "Herramienta integrada para la gestión eficiente de infraestructuras viarias basada en el empleo de recursos geotérmicos (project ref.: PID2022-142097OA-I00). In addition, S.B.C and M.G.MA. acknowledge the grants RYC2021-034720-I and RYC2021-034813-I, respectively, funded by the Ministry of Science and Innovation MCIN/AEI/10.13039/501100011033 and by the European Union "NextGenerationEU"/PRTR. The authors would also like to thank the TIDOP Research Group of the Department of Cartographic and Land Engineering of the Higher Polytechnic School of Ávila (University of Salamanca).

Conflicts of Interest: The authors declare no conflicts of interest.

Nomenclature

Acronyms

4GDH	4th Generation District Heating
5GDH	5th Generation District Heating
ASA	Acrylonitrile Styrene Acrylate
CI	Confidence Interval
COP	Coefficient of Performance
DH	District heating
GHG	Greenhouse Gas Emissions
HDT	Heat Deflection Temperature
PCV	Polyvinyl chloride
SD	Standard Deviation

Formulae

r_e	Recovery efficiency
σ	Standard Deviation
A	Surface área, m^2
C_p	Specific heat capacity, J/kg·K, J/g·°C
D	Diameter, m
D_1	Internal pipe diameter, m
D_2	External pipe diameter, m
h	Convective heat transfer coefficient, $W/m^2 \cdot k$
ha	Convective coefficient for air, $W/m^2 \cdot k$
hw	Convective coefficient for water, $W/m^2 \cdot k$
k	Thermal conductivity, W/m·K
ρ	Density, kg/m^3
η	Viscosity, kg/m·s
L	Length, m
$\dot{m}$	Mass flow, kg/s
N	number of data points in the population
Q	Heat transfer, W
Q_{loss}	Amount of heat lost, W
$Q_{recovered}$	Recovered heat, W
Q_{return}	Heat of the return water, W
Q_{total}	Total heat supplied to the system, W

q	Heat transfer per unit of pipe length, W/m
r	Radius, m
r_o	Outer radius of the inner pipe, m
r_i	Inner radius of the outer pipe, m
U	Overall heat transfer coefficient, W/m^2·K
T	Temperature, °C, K
ΔT	Temperature difference between the inlet and outlet fluids, °C, K
$T_{ambient}$, T_a	Ambient temperature, °C, K
T_{return}	Temperature of the return water, °C, K
T_1	Internal pipe temperature, °C, K
T_2	External pipe temperature, °C, K
x_i	Data point
$\overline{x}$	Population mean
$z_{\alpha/2}$	Critical value of confidence level

References

1. Delivering the European Green Deal—European Commission. Available online: https://commission.europa.eu/strategy-and-policy/priorities-2019-2024/european-green-deal/delivering-european-green-deal_en (accessed on 5 July 2024).
2. Recovery Plan for Europe—European Commission. Available online: https://commission.europa.eu/strategy-and-policy/recovery-plan-europe_en (accessed on 5 July 2024).
3. Energy efficiency in buildings. Available online: https://commission.europa.eu/document/download/65660913-cecb-4f2f-b34c-c9bbf9bed1af_en?filename=in_focus_energy_efficiency_in_buildings_en.pdf&prefLang=es (accessed on 5 July 2024).
4. Abugabbara, M.; Gehlin, S.; Lindhe, J.; Axell, M.; Holm, D.; Johansson, H.; Larsson, M.; Mattsson, A.; Näslund, U.; Puttige, A.R.; et al. How to develop fifth-generation district heating and cooling in Sweden? Application review and best practices proposed by middle agents. *Energy Rep.* **2023**, *9*, 4971–4983. [CrossRef]
5. Santamouris, M. Cooling the buildings—Past, present and future. *Energy Build.* **2016**, *128*, 617–638. [CrossRef]
6. Munćan, V.; Mujan, I.; Macura, D.; Anđelković, A.S. The state of district heating and cooling in Europe—A literature-based assessment. *Energy* **2024**, *304*, 132191. [CrossRef]
7. Directive (EU) 2023/1791 of the European Parliament and of the Council of 13 September 2023 on Energy Efficiency and Amending Regulation (EU) 2023/955 (Recast) (Text with EEA Relevance). 2023, Volume 231. Available online: http://data.europa.eu/eli/dir/2023/1791/oj/eng (accessed on 5 July 2024).
8. Communication from the Commission to the European Parliament, the Council, the European Economic and Social Committee and the Committee of the Regions an EU Strategy on Heating and Cooling. 2016. Available online: https://eur-lex.europa.eu/legal-content/EN/TXT/?qid=1575551754568&uri=CELEX:52016DC0051 (accessed on 5 July 2024).
9. Werner, S. International review of district heating and cooling. *Energy* **2017**, *137*, 617–631. [CrossRef]
10. Lund, H.; Østergaard, P.A.; Nielsen, T.B.; Werner, S.; Thorsen, J.E.; Gudmundsson, O.; Arabkoohsar, A.; Mathiesen, B.V. Perspectives on fourth and fifth generation district heating. *Energy* **2021**, *227*, 120520. [CrossRef]
11. Buffa, S.; Cozzini, M.; D'Antoni, M.; Baratieri, M.; Fedrizzi, R. 5th generation district heating and cooling systems: A review of existing cases in Europe. *Renew. Sustain. Energy Rev.* **2019**, *104*, 504–522. [CrossRef]
12. Sáez Blázquez, C.; Farfán Martín, A.; Nieto, I.M.; González-Aguilera, D. Economic and Environmental Analysis of Different District Heating Systems Aided by Geothermal Energy. *Energies* **2018**, *11*, 1265. [CrossRef]
13. Blázquez, C.S.; Verda, V.; Nieto, I.M.; Martín, A.F.; González-Aguilera, D. Analysis and optimization of the design parameters of a district groundwater heat pump system in Turin, Italy. *Renew. Energy* **2020**, *149*, 374–383. [CrossRef]
14. Gudmundsson, O.; Thorsen, J.E. Source-to-sink efficiency of blue and green district heating and hydrogen-based heat supply systems. *Smart Energy* **2022**, *6*, 100071. [CrossRef]
15. Mi, P.; Zhang, J.; Han, Y.; Guo, X. Study on energy efficiency and economic performance of district heating system of energy saving reconstruction with photovoltaic thermal heat pump. *Energy Convers. Manag.* **2021**, *247*, 114677. [CrossRef]
16. Sun, F.; Zhao, X.; Chen, X.; Fu, L.; Liu, L. New configurations of district heating system based on natural gas and deep geothermal energy for higher energy efficiency in northern China. *Appl. Therm. Eng.* **2019**, *151*, 439–450. [CrossRef]
17. Reiners, T.; Gross, M.; Altieri, L.; Wagner, H.-J.; Bertsch, V. Heat pump efficiency in fifth generation ultra-low temperature district heating networks using a wastewater heat source. *Energy* **2021**, *236*, 121318. [CrossRef]
18. Zajacs, A.; Bogdanovics, R.; Borodinecs, A. Analysis of low temperature lift heat pump application in a district heating system for flue gas condenser efficiency improvement. *Sustain. Cities Soc.* **2020**, *57*, 102130. [CrossRef]
19. Prokhorenkov, A.M.; Saburov, I.V.; Sovlukov, A.S.; Viktorov, V.A. Efficiency Increase of District Heating Plants through Application of Cost-Oriented Control and Monitoring Means. *IFAC Proc. Vol.* **2001**, *34*, 127–131. [CrossRef]
20. Song, J.; Li, W.; Zhu, S.; Zhou, C.; Xue, G.; Wu, X. Predicting hourly heating load in district heating system based on the hybrid Bi-directional long short-term memory and temporal convolutional network model. *J. Clean. Prod.* **2024**, *463*, 142769. [CrossRef]
21. Boussaid, T.; Rousset, F.; Scuturici, V.-M.; Clausse, M. Enabling fast prediction of district heating networks transients via a physics-guided graph neural network. *Appl. Energy* **2024**, *370*, 123634. [CrossRef]

22. Guo, T.; Chen, Y.; Kriegel, M. Novel multi-level optimization of district heating systems: Managing spatial scale and equipment portfolio design. *Energy Build.* **2024**, *317*, 114395. [CrossRef]
23. Wack, Y.; Sollich, M.; Salenbien, R.; Diriken, J.; Baelmans, M.; Blommaert, M. A multi-period topology and design optimization approach for district heating networks. *Appl. Energy* **2024**, *367*, 123380. [CrossRef]
24. Wirtz, M.; Heleno, M.; Romberg, H.; Schreiber, T.; Müller, D. Multi-period design optimization for a 5th generation district heating and cooling network. *Energy Build.* **2023**, *284*, 112858. [CrossRef]
25. Sarma, U.; Karnitis, G.; Zuters, J.; Karnitis, E. District heating networks: Enhancement of the efficiency. *Insights Reg. Dev.* **2019**, *1*, 200–213. [CrossRef]
26. Zohuri, B. *Heat Pipe Design and Technology: A Practical Approach*; Springer: Cham, Switzerland, 2011.
27. Aresti, L.; Christodoulides, P.; Florides, G. A review of the design aspects of ground heat exchangers. *Renew. Sustain. Energy Rev.* **2018**, *92*, 757–773. [CrossRef]
28. Javadi, H.; Mousavi Ajarostaghi, S.; Rosen, M.; Pourfallah, M. Performance of ground heat exchangers: A comprehensive review of recent advances. *Energy* **2019**, *178*, 207–233. [CrossRef]
29. Wrzalik, A. Innovative Solutions in the Process of Heat Supply. *Qual. Prod. Improv.—QPI* **2019**, *1*, 155–161. [CrossRef]
30. Mukhametrakhimov, R.; Galautdinov, A.; Panchenko, A.; Gorbunova, T. Improving the quality of installation of preinsulated pipelines of heat supply systems. *E3S Web Conf.* **2021**, *264*, 02068. [CrossRef]
31. Geertsen, C.; Langford, S.; McKinnon, C.; McKinnon, F.; Niesen, V.; Orberg, F.; Wang, N. Challenges of Engineering the Hottest Subsea Heated Pipeline for the CRISP Project. In Proceedings of the Offshore Technology Conference, Houston, TX, USA, 16–19 August 2021.
32. Davydov, S.Y.; Makarov, V.N.; Kozhushko, G.G.; Makarov, N.V.; Ugolnikov, A.V. Innovative Method of Active Heat Protection of Pipelines for Moving Hot Bulk Materials and Cylindrical Apparatuses. *Refract. Ind. Ceram.* **2022**, *62*, 618–622. [CrossRef]
33. Wang, Y.; Qi, C.; Ding, Z.; Tu, J.; Zhao, R. Numerical simulation of flow and heat transfer characteristics of nanofluids in built-in porous twisted tape tube. *Powder Technol.* **2021**, *392*, 570–586. [CrossRef]
34. Ghazi, T.; Attar, M.R.; Ghorbani, A.; Alshihmani, H.; Davoodi, A.; Passandideh-Fard, M.; Sardarabadi, M. Synergistic effect of active-passive methods using fins surface roughness and fluid flow for improving cooling performance of heat sink heat pipes. *Exp. Heat Transf.* **2024**, *37*, 649–664. [CrossRef]
35. Zhang, D.; Jiang, E.; Zhou, J.; Shen, C.; He, Z.; Xiao, C. Investigation on enhanced mechanism of heat transfer assisted by ultrasonic vibration. *Int. Commun. Heat Mass Transf.* **2020**, *115*, 104523. [CrossRef]
36. *D792*; Standard Test Methods for Density and Specific Gravity (Relative Density) of Plastics by Displacement. ASTM International: West Conshohocken, PA, USA, 2020.
37. *UNE-EN ISO 527-1:2020*; Plastics—Determination of tensile properties—Part 1: General principles (ISO 527-1:2019). Asociación Española de Norma-lización: Madrid, Spain, 2020.
38. *UNE-EN ISO 178:2020*; Plastics—Determination of flexural properties (ISO 178:2019). Asociación Española de Normalización: Madrid, Spain, 2020.
39. *UNE-EN ISO 179-1:2024*; Plastics—Determination of Charpy impact properties—Part 1: Non-instrumented impact test (ISO 179-1:2023). Asociación Española de Normalización: Madrid, Spain, 2024.
40. *UNE-ISO 7619-1:2011*; Rubber, vulcanized or thermoplastic—Determination of indentation hardness—Part 1: Durometer method (Shore hardness). Asociación Española de Normalización: Madrid, Spain, 2011.
41. *UNE-EN ISO 11357-2:2021*; Plastics—Differential scanning calorimetry (DSC)—Part 2: Determina-tion of glass transition temperature and step height (ISO 11357-2:2020). Asociación Española de Normalización: Madrid, Spain, 2021.
42. *UNE-EN ISO 308:1998*; Plastics—Phenolic Moulding Materials—Determination of Acetone-Soluble Matter (Apparent Resin Content of Material in the Unmoulded State). Asociación Española de Normalización: Madrid, Spain, 1998.
43. *UNE-EN ISO 75-1:2020*; Plastics—Determination of temperature of deflection under load—Part 1: General test method (ISO 75-1:2020). Asociación Española de Normalización: Madrid, Spain, 2020.
44. Nuño-Villanueva, N.; Maté-González, M.Á.; Nieto, I.M.; Blázquez, C.S.; Martín, A.F.; González-Aguilera, D. GIS-based selection methodology for viable District Heating areas in Castilla y León, Spain. *Geothermics* **2023**, *113*, 102767. [CrossRef]
45. ASTM-E220 | Standard Test Method for Calibration of Thermocouples By Comparison Techniques | Document Center, Inc. Available online: https://www.document-center.com/standards/show/ASTM-E220 (accessed on 5 July 2024).
46. Medidor de Caudal PCE-TDS 200 M | PCE Instruments. Available online: https://www.pce-instruments.com/espanol/instrumento-medida/medidor/medidor-de-caudal-pce-instruments-medidor-de-caudal-pce-tds-200-m-det_6190325.htm?_list=kat&_listpos=1 (accessed on 4 November 2024).
47. Schmidt, D.; Lygnerud, K.; Werner, S.; Geyer, R.; Schrammel, H.; Østergaard, D.S.; Gudmundsson, O. Successful implementation of low temperature district heating case studies. *Energy Rep.* **2021**, *7*, 483–490. [CrossRef]
48. Fonseca, J.A.; Schlueter, A. Integrated model for characterization of spatiotemporal building energy consumption patterns in neighborhoods and city districts. *Appl. Energy* **2015**, *142*, 247–265. [CrossRef]
49. Li, H.; Nord, N. Transition to the 4th generation district heating—Possibilities, bottlenecks, and challenges. *Energy Procedia* **2018**, *149*, 483–498. [CrossRef]
50. Yıldırım, N.; Toksoy, M.; Gökçen, G. District heating system design for a university campus. *Energy Build.* **2006**, *38*, 1111–1119. [CrossRef]

51. Kakac, S.; Yener, Y.; Naveira-Cotta, C.P. *Heat Conduction, Fifth Edition*, 5th ed.; CRC Press: Boca Raton, FL, USA, 2018; ISBN 978-1-315-17871-4.
52. Beier, R.A.; Acuña, J.; Mogensen, P.; Palm, B. Transient heat transfer in a coaxial borehole heat exchanger. *Geothermics* **2014**, *51*, 470–482. [CrossRef]
53. Esbjerg Heat Pump. MAN Energy Solutions. Available online: https://www.man-es.com/discover/esbjerg-heat-pump (accessed on 19 July 2024).
54. Calculadoras. Ministerio para la Transición Ecológica y el Reto Demográfico. Available online: https://www.miteco.gob.es/es/cambio-climatico/temas/mitigacion-politicas-y-medidas/calculadoras.html (accessed on 19 July 2024).
55. OMIE. Available online: https://www.omie.es/ (accessed on 19 July 2024).